J. Huang, J.D. Biggs, Y. Bai, N. Cui
Integrated Guidance and Control for Solar Sail Station-Keeping with Optical Degradation
Advances in Space Research, In press - Published online 29/01/2020
doi:10.1016/j.asr.2020.01.010

Integrated guidance and control for solar sail station-keeping with optical degradation

Jia Huang[a,b], James D. Biggs[c], Yuliang Bai[a,*], Naigang Cui[a]

[a] *School of Astronautics, Harbin Institute of Technology, Harbin 150001, China*
[b] *Institute of Systems Engineering, China Academy of Engineering Physics, Mianyang 621999, China*
[c] *Department of Aerospace Science and Technology, Politecnico di Milano, Milano 20156, Italy*

Abstract

Current control approaches for solar sail station-keeping on libration point orbits have not considered the degradation of the sail's optical properties. However, significant optical degradation could lead to poor station-keeping performance or even complete failure. This paper presents an integrated guidance and control strategy to address this problem by updating the reference orbit based on in-situ estimation. An exponential optical degradation model is incorporated into the solar radiation acceleration model, and an on-line reference orbit update approach is incorporated into the station-keeping, coupled with an active disturbance rejection controller. The reflection coefficient is estimated on-line and the reference orbit is updated discretely when the optical properties have degraded by a prescribed amount. This strategy provides discrete updates to the reference orbits such that the perturbation due to the optical degradation is maintained within a small range. These smaller perturbations can be dealt with by the controller's robustness and station-keeping can be sustained for long durations even in the presence of large optical degradation.

Keywords: Solar sail, Station-keeping, Optical degradation, Integrated guidance and control, Reference orbit update

*Corresponding author
Email addresses: caep_huangjia@163.com (Jia Huang), jamesdouglas.biggs@polimi.it (James D. Biggs), baiyuliang@hit.edu.cn (Yuliang Bai), cui_naigang@163.com (Naigang Cui)

1. Introduction

A solar sail is a type of spacecraft which uses solar radiation pressure (SRP) to generate continuous and unlimited propulsion. In addition, solar sails have the potential to enable completely new orbits that are different from the orbits found in the classical two-body problem and restricted three-body problem. These orbits can enable completely new mission applications such as polar observation (Gong and Li, 2014; Macdonald et al., 2006; Ceriotti and McInnes, 2012; Heiligers et al., 2019; Grebow et al., 2010), displaced geostationary orbits (Heiligers et al., 2012) and early solar storm warnings (McInnes, 1999; Yen, 2004; Heiligers et al., 2014). Each of these applications requires station-keeping to maintain the unstable reference orbits (Biggs et al., 2009; Lawrence and Piggott, 2004; Baoyin and McInnes, 2005; Waters and McInnes, 2008). Critically, the reference orbits in these solar sail applications have been designed based on an assumption that the optical properties are known and constant or by using a perfectly reflecting SRP model. However, in reality, the optical properties cannot be modelled accurately. Moreover, the optical properties degrade with time due to the erosive effects of the harsh space environment (Dachwald et al., 2006, 2007). These errors in the optical properties can yield poor station-keeping performance (or even complete failure of the spacecraft to track the reference trajectory).

A solar sail using only the sail angles as the control variables for station-keeping cannot adequately compensate for the errors in the optical properties (Huang et al., 2019). Moreover, the errors in the optical properties mainly affect the magnitude of the SRP acceleration, while this cannot be controlled effectively by varying the sail angles only. The controllability of the magnitude of SRP acceleration can be improved by introducing reflectivity control devices (RCDs) (Funase et al., 2011; Gong et al., 2014; Biggs and Negri, 2019; Negri and Biggs, 2019). This technology has been demonstrated as an attitude control actuation system for JAXA's small solar power sail demonstrator "IKAROS".

RCDs are able to control the magnitude of SRP acceleration by switching the optical properties between two states (Funase et al., 2011), for example, between specular reflection and diffusion. Therefore, RCDs can compensate for the perturbed acceleration induced by the errors in the optical properties to some extent. In other words, RCDs can improve the robustness to the errors in the optical properties. However, the available control acceleration of RCDs is highly constrained since RCDs usually account for only a small ratio of the whole sail surface (since RCDs are far heavier than typical sail materials). For example, the RCDs of "IKAROS" only account for 9.2% of the whole sail surface (Funase et al., 2011). Therefore, an RCD solar sail is only able to provide robustness to optical degradation over short duration missions. With large optical degradation in long duration missions it may not be possible to maintain the reference orbit.

To address this problem, this paper presents an integrated guidance and control strategy for the long duration station-keeping of an RCD solar sail in the presence of optical degradation. This strategy is inspired by the idea in Biggs and Ciccarelli (2019), where the SRP acceleration is estimated as a disturbance using an extended state observer (ESO) based on a perfectly reflecting SRP model, and then the artificial equilibrium point (the reference orbit) is updated. In this paper, instead of estimating the SRP acceleration, the reflection coefficient is estimated on-line based on a non-perfectly reflecting SRP model using a direct algorithm, which is significantly faster and avoids the slow convergence which occurs with large initial estimation errors when using an ESO. The reference orbit will be updated using numerical continuation (Howell, 1984; Heiligers et al., 2016) when the optical properties have degraded by a prescribed amount. These discrete corrections to the reference orbit are able to keep the perturbation due to the errors in the optical properties in a small range, such that the requirement for the robustness of station-keeping to the errors in the optical properties is significantly reduced.

To demonstrate this approach, station-keeping simulations for halo orbits in the Sun-Earth circular restricted three-body problem (CRTBP) are performed.

An exponential optical degradation model taking into account solar radiation dose (Dachwald et al., 2006, 2007) is incorporated into the SRP model. A non-linear active disturbance rejection control (ADRC) (Han, 2008, 2009) is used for the station-keeping control, coupled with the on-line reference orbit update algorithm. The results show that this approach is able to maintain the station-keeping performance in the presence of large optical degradation, and significantly extend the mission time compared to the station-keeping without reference orbit update.

2. Solar sail dynamics with optical degradation

The equations of motion in the Sun-Earth CRTBP for a non-perfectly reflecting solar sail covered, in part, with RCDs is presented. In addition, the exponential optical degradation model proposed by Dachwald et al. (2006, 2007) is incorporated into the SRP acceleration model.

2.1. Equations of motion

The equations of motion are expressed in a rotating frame as shown in Fig. 1, where the origin is at the Sun-Earth barycenter, the x-axis points in the direction of the Earth, the z-axis is the axis of the rotation of the Sun-Earth system, and the y-axis completes the triad. In addition, the Sun-Earth distance, the frame's angular velocity, and the mass of the Sun-Earth system are normalized to unity.

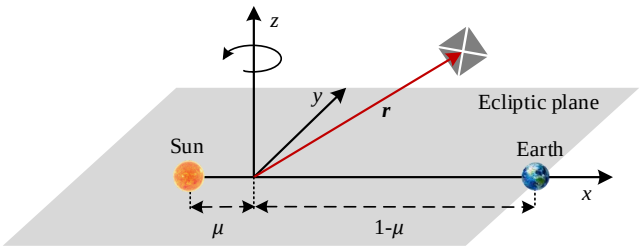

Figure 1: The rotating reference frame

The vectorial form of the equations of motion is given by

$$\ddot{\boldsymbol{r}} + 2\boldsymbol{\omega} \times \dot{\boldsymbol{r}} = \nabla U + \boldsymbol{a} \tag{1}$$

where $\boldsymbol{r} = [x, y, z]^T$ is the non-dimensionalized solar sail position vector, $\boldsymbol{\omega} = [0, 0, 1]^T$ is the non-dimensionalized angular velocity of the rotating frame, and $\boldsymbol{a}$ is the non-dimensionalized SRP acceleration. The potential function U is given by

$$U = \frac{1}{2}(x^2 + y^2) + \frac{1-\mu}{r_1} + \frac{\mu}{r_2} \tag{2}$$

where μ is the ratio of the smaller primary mass to the total mass of the two primaries, which for the Sun-Earth system is $\mu = 3.04 \times 10^{-6}$. Finally, r_1 and r_2 are the non-dimensionalized distances from the solar sail to the first and the second primary, respectively.

The non-dimensionalized SRP acceleration model of a non-perfectly reflecting solar sail is given by Eq. (3), which takes into account the specular reflection, diffuse reflection, absorption, and emission (McInnes, 1999; Dachwald et al., 2006), that is

$$\boldsymbol{a} = \beta \frac{1-\mu}{2r_1^2} (\boldsymbol{s} \cdot \boldsymbol{n}) \left[(1 - s\rho)\boldsymbol{s} + \left(2s\rho (\boldsymbol{s} \cdot \boldsymbol{n}) + (1-s)\rho B_f + (1-\rho) \frac{\varepsilon_f B_f - \varepsilon_b B_b}{\varepsilon_f + \varepsilon_b} \right) \boldsymbol{n} \right] \tag{3}$$

where $\boldsymbol{n}$ is the unit vector normal to the sail, $\boldsymbol{s} = [x + \mu, y, z]^T / r_1$ is the unit vector of the Sun-sail line, β is the lightness number, ρ is the reflection coefficient, s denotes the ratio of the specular reflection to the total reflection, ε_f and ε_b are the front and back emissivities, and B_f and B_b are the front and back non-Lambertian coefficients. Therefore, the SRP acceleration model is parameterized by six optical coefficients, that is, $\Theta = \{\rho, s, \varepsilon_f, \varepsilon_b, B_f, B_b\}$. In this paper, two values for β are considered. One is 0.056, which is a typical value of β for early solar storm warnings (McInnes, 1999), and it is equivalent to 0.05 in the case of a perfectly reflecting sail, a value typically used in the literature (Biggs et al., 2011, 2009; Biggs and McInnes, 2009). In addition, $\beta = 0.028$ is

also considered as an additional case to compare the results. This is a nearer term value, which is closer to the current technology readiness level.

The unit vector $\boldsymbol{n}$ can be expressed using two sail angles (a pitch angle γ and an azimuth angle δ), which are two control variables for station-keeping, that is

$$\boldsymbol{n} = [\cos\gamma\cos\delta,\ \cos\gamma\sin\delta,\ \sin\gamma]^T \tag{4}$$

The RCDs considered in this paper can switch between a specular state, in which most of the photons are specularly reflected, and a diffuse state, in which most of the photons are diffusely reflected. For the diffuse state, it is assumed that all the specular reflection transforms to diffuse reflection, i.e. $s = 0$. The optical properties of the sail surface without RCDs are assumed to be the same as those of the RCDs in the specular state. We define the RCD ratio σ (another control variable for station-keeping) as the ratio of the area of the RCDs in the diffusive state to the total sail area. Therefore, according to the different optical properties, the total SRP acceleration can be divided into the following two parts:

$$\boldsymbol{a} = \boldsymbol{a}_1 + \boldsymbol{a}_2 \tag{5}$$

$$\boldsymbol{a}_1 = (1-\sigma)\,\beta\frac{1-\mu}{2r_1^2}\,(\boldsymbol{s}\cdot\boldsymbol{n})\left[(1-s\rho)\boldsymbol{s} + \left(2s\rho\,(\boldsymbol{s}\cdot\boldsymbol{n}) + (1-s)\rho B_f + (1-\rho)\frac{\varepsilon_f B_f - \varepsilon_b B_b}{\varepsilon_f + \varepsilon_b}\right)\boldsymbol{n}\right] \tag{6}$$

$$\boldsymbol{a}_2 = \sigma\beta\frac{1-\mu}{2r_1^2}\,(\boldsymbol{s}\cdot\boldsymbol{n})\left[\boldsymbol{s} + \left(\rho B_f + (1-\rho)\frac{\varepsilon_f B_f - \varepsilon_b B_b}{\varepsilon_f + \varepsilon_b}\right)\boldsymbol{n}\right] \tag{7}$$

where $\boldsymbol{a}_1$ is the SRP acceleration generated by the RCDs in the specular state and the sail surface without RCDs, while $\boldsymbol{a}_2$ is the SRP acceleration generated by the RCDs in the diffusive state.

In this paper, we consider a class of reference orbits such that the sail normal is directed along the Sun-sail line, that is, $\boldsymbol{s} = \boldsymbol{n}$. Therefore, when designing a

reference orbit, Eqs. (5–7) can be expressed in the corresponding reduced form:

$$\boldsymbol{a} = \beta K \frac{1-\mu}{r_1^2}\boldsymbol{n} \tag{8}$$

$$K(\Theta,\sigma) = \frac{1}{2}\left[(1-\rho)\frac{\varepsilon_f B_f - \varepsilon_b B_b}{\varepsilon_f + \varepsilon_b} + s\rho\,(1-\sigma)\,(1-B_f) + 1 + \rho B_f\right] \tag{9}$$

where K can be considered as an efficiency factor that depends on the optical coefficients Θ and the RCD ratio σ.

The parameters for the reference orbit are called nominal parameters, and are denoted by a subscript e, such as $K_e = K(\Theta_e, \sigma_e)$. The values of Θ_e are taken from Heaton et al. (2017), that is, $\Theta_e = \{\rho = 0.91, s = 0.89, \varepsilon_f = 0.025, \varepsilon_b = 0.27, B_f = 0.79, B_b = 0.67\}$. The maximum σ equates to the proportion of area covered by RCDs to the area of the whole sail surface. In theory, the larger the maximum value of σ, the more control authority there is to vary the acceleration of the sail. However, from the view of real applications, since RCDs are far heavier than typical sail materials, the maximum σ should be as small as possible while maintaining the necessary control authority. In this paper, $\sigma_{\max} = 0.2$ is assumed, which is proved to be a moderate value for station-keeping according to the simulation results. Furthermore, the nominal value for σ is set to 0.1, i.e., half of the RCDs are in the specular state for the nominal state of the solar sail, and the maximum deviation of σ is ± 0.1.

2.2. Optical degradation model

In this paper, the exponential optical degradation model, which takes into account the solar radiation dose (SRD) (Dachwald et al., 2006, 2007), is considered, that is

$$\frac{p(t)}{p_0} = \begin{cases} (1 + de^{-\lambda\Sigma(t)})/(1+d) & \text{for} \quad p \in \{\rho, s\} \\ 1 + d(1 - e^{-\lambda\Sigma(t)}) & \text{for} \quad p = \varepsilon_f \\ 1 & \text{for} \quad p \in \{\varepsilon_b, B_f, B_b\} \end{cases} \tag{10}$$

where p denotes a generic optical coefficient. The parameter d is a degradation factor parameterizing the maximum variation in p, and $\lambda = \ln 2/\hat{\Sigma}$ is a degradation constant parameterizing the rate of degradation, where $\hat{\Sigma}$ is the relative SRD when $p = (p_0 + p_\infty)/2$, where the subscripts 0 and ∞ denote the initial time and the moment after infinite time, respectively. Finally, $\Sigma(t)$ is the relative SRD, which can be computed by

$$\dot{\Sigma}(t) = r_0^2 \cos\alpha / r^2 \tag{11}$$

where $r_0 = 1$ AU is the distance between the Sun and the Earth, r is the distance between the Sun and the sail, and α is the angle between the sail normal and the Sun-sail line.

In this paper, d is set to 0.05, and $\hat{\Sigma}$ is set to 5. It should be noted that the systematic measurement data for the optical degradation of solar sails is not known. Therefore, the chosen values for the degradation parameters are only used to illustrate the presented integrated guidance and control strategy as an example. If the real degradation is slower than that in this paper, the presented strategy will still be effective, while if the real degradation is faster, additional simulations should be performed.

Equation (10) implies that ρ and s decrease with time, while ε_f increases with time, with all the other coefficients being constant. Figure 2 shows the variation of the three optical coefficients with time. Although the variation rates of the three coefficients are of the same order of magnitude, the impacts of them on the SRP acceleration are different. Since the reflection usually accounts for a vast majority of the SRP acceleration, the degradation of ρ is the major factor affecting the SRP acceleration. This can be indicated by the partial derivatives of K with respect to the three coefficients. For example, $\partial K/\partial\rho|_{K=K_e} \approx 1.2$, $\partial K/\partial s|_{K=K_e} \approx 0.17$, and $\partial K/\partial\varepsilon_f|_{K=K_e} \approx 0.12$ in this paper. Therefore, the influence of the variation of ρ is one order of magnitude larger than those of the variations of s and ε_f.

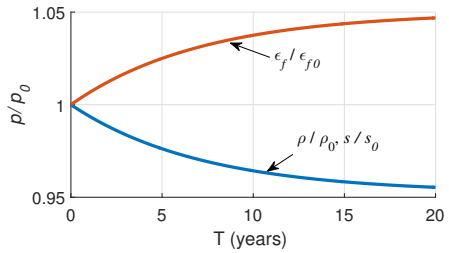

Figure 2: Variation of the optical coefficients with time

3. On-line reference orbit update

The key concept of the presented integrated guidance and control strategy is to estimate the reflection coefficient ρ on-line and, then, update the reference orbit when the optical properties have degraded to a significant extent. We assume that the sail can effectively track the reference orbit when the errors in the optical properties are within an acceptable range. This assumption is reasonable since the controller has a certain degree of robustness to overcome small errors. Therefore, when the sail is effectively tracking the current reference orbit, the orbit states and the SRP acceleration can be considered to be approximately equal to their nominal values for the current reference orbit. Thus, from Eq. (8), the real K will be approximately equal to its nominal value, that is

$$K(\Theta, \sigma) = K_e \tag{12}$$

In Eq. (12), K_e and σ are known, while Θ, which includes six coefficients, is unknown. Recall that in Section 2 it was demonstrated that a variation in ρ has a considerably larger effect on K than the other coefficients. Therefore, it is reasonable to neglect the influence of the errors in the other optical coefficients in order to develop a simple estimation procedure. With such an assumption ρ can be estimated by solving Eq. (12), to give

$$\hat{\rho} = \left(2K_e - \frac{\varepsilon_f B_f - \varepsilon_b B_b}{\varepsilon_f + \varepsilon_b} - 1\right) \Bigg/ \left(s\,(1-\sigma)\,(1-B_f) + B_f - \frac{\varepsilon_f B_f - \varepsilon_b B_b}{\varepsilon_f + \varepsilon_b}\right) \tag{13}$$

where $\hat{\rho}$ is the estimated value for ρ. Although the errors in the other optical coefficients will lead to an estimation error in $\hat{\rho}$, this error is small enough to be compensated for by the closed-loop control. When $\hat{\rho}$ is obtained, K_e can be updated by substituting $\hat{\rho}$ and σ_e into Eq. (9), and then the reference orbit can be updated using numerical continuation (Howell, 1984; Heiligers et al., 2016) with K_e as the continuation parameter.

Since K_e is constant, and Θ and σ are the two time-varying parameters in Eq. (12), it follows that σ always changes with changes in Θ, that is, the degradation of Θ can be characterized by σ. In Section 5 it will be shown that σ decreases with the degradation of Θ. Within the integrated guidance and control strategy, an update to the reference trajectory is performed after a significant amount of optical degradation, explicitly when σ reduces below a prescribed value σ^*, i.e. $\sigma < \sigma^*$. However, the specific value for σ^* depends on several factors which will be analyzed in the following sections.

Figure 3 shows the flow chart of the integrated guidance and control strategy, where $\boldsymbol{X}_e$ is the reference orbit state. When $\sigma < \sigma^*$, the reference orbit will be updated, otherwise, the station-keeping still uses the current reference orbit.

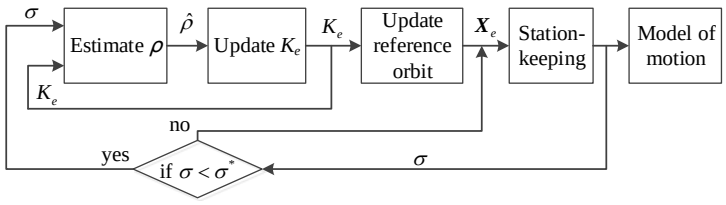

Figure 3: Flow chart of the integrated guidance and control strategy

It should be noted that the numerical continuation with K_e can generate three different families of orbits by keeping the initial x, z, or v_y constant, where v_y is the velocity in the y-direction. Taking the case of $\beta = 0.056$ as an example, the three families of orbit are shown in Figs. 4–6.

In Fig. 4, as K_e decreases, the amplitude of the orbits increases significantly (the maximum variation of amplitude is 0.0068 AU in the z-direction, see the 3rd subfigure in Fig. 4), whereas the variation of the amplitude of the orbits in

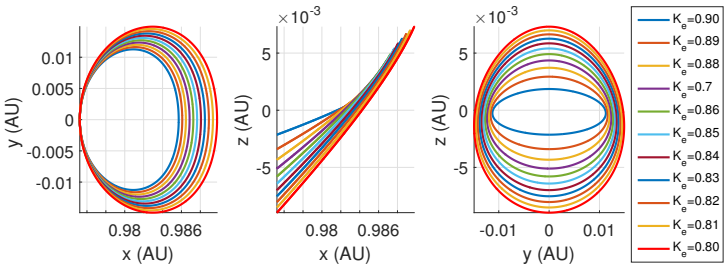

Figure 4: Family of orbits with fixed initial x

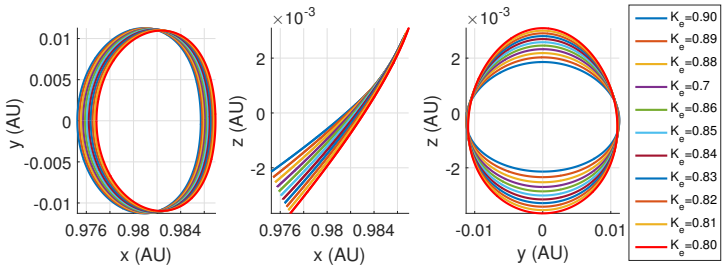

Figure 5: Family of orbits with fixed initial v_y

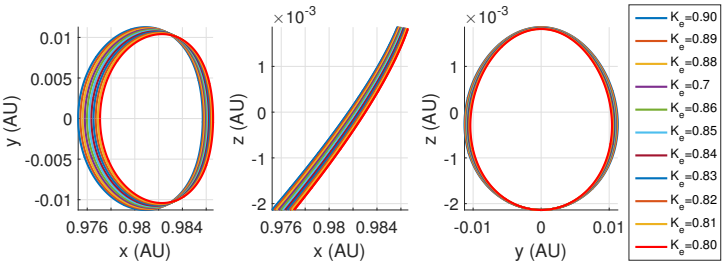

Figure 6: Family of orbits with fixed initial z

Fig. 6 is much smaller. Specifically, the maximum variation of the amplitude is 8.5×10^{-4} AU in the y-direction (see the 3rd subfigure in Fig. 6), while the orbits move towards the Earth by 0.002 AU (see the 2nd subfigure in Fig. 6). The maximum variation of the orbits in Fig. 5 is 0.0015 AU in the z-direction, which is between those in Fig. 4 and Fig. 6. Therefore, the orbits in Fig. 4 are the most sensitive to K_e, while the orbits in Fig. 6 are the least sensitive to K_e, that is, with the same variation in K_e, the orbits in Fig. 6 will vary least

among the three families.

A problem encountered when updating the reference orbit in-situ is that the new reference orbit may be far from the current reference orbit, and thus a large orbit error will arise when maneuvering between reference orbits. In this case, the station-keeping may fail due to this large error. Therefore, the family of orbits whose amplitude variation is less sensitive to K_e are more suitable as reference orbits. Thus, in this paper the family of orbits in Fig. 6 are used as the reference orbits.

4. Nonlinear active disturbance rejection station-keeping control

Theoretically, the presented integrated guidance and control strategy does not rely on a particular type of control law. Indeed, this strategy could utilize either a simple proportional or an LQR controller. However, as mentioned in Section 3, a large orbit error can arise when the reference orbit is updated. Moreover, the estimation of the reflection coefficient relies on the assumption that the steady-state orbit error is approximately equal to zero. Therefore, it is critical that the selected control law should: i) be robust to large orbit errors, and ii) have a high precision tracking capability such that the steady-state error is as small as possible. However, there is usually a trade-off between these two objectives when using linear control laws. In this paper, a nonlinear active disturbance rejection control (ADRC) law (Han, 2008, 2009) is used for the station-keeping, which can achieve both these objectives without the need to trade one off against the other.

4.1. System model for ADRC station-keeping control

The equations of motion in Eq. (1) can be transformed into the following form

$$\begin{aligned} \dot{\boldsymbol{r}} &= \boldsymbol{v} \\ \dot{\boldsymbol{v}} &= \boldsymbol{f}(\boldsymbol{r}, \boldsymbol{v}) + \boldsymbol{a} \end{aligned} \tag{14}$$

where $\boldsymbol{v} = [v_x, v_y, v_z]^T$ is the velocity vector and $\boldsymbol{f} = \nabla U - 2\boldsymbol{\omega} \times \boldsymbol{v}$ is the nonlinear dynamics.

The deviation equations of motion relative to the reference orbit are used as the system model for control design, that is

$$\begin{aligned} \Delta\dot{\boldsymbol{r}} &= \Delta\boldsymbol{v} \\ \Delta\dot{\boldsymbol{v}} &= \Delta\boldsymbol{f}(\boldsymbol{r}, \boldsymbol{v}) + \boldsymbol{d} + \Delta\boldsymbol{a} \end{aligned} \tag{15}$$

where $\Delta\boldsymbol{r} = \boldsymbol{r} - \boldsymbol{r}_e$, $\Delta\boldsymbol{v} = \boldsymbol{v} - \boldsymbol{v}_e$, $\Delta\boldsymbol{f} = \boldsymbol{f}(\boldsymbol{r}, \boldsymbol{v}) - \boldsymbol{f}(\boldsymbol{r}_e, \boldsymbol{v}_e)$, and $\Delta\boldsymbol{a} = \boldsymbol{a} - \boldsymbol{a}_e$ are the deviations from the reference orbit, whereas $\boldsymbol{d}$ is the disturbance due to the error in optical properties.

The total disturbance $\boldsymbol{w}$ is given by $\Delta\boldsymbol{f}$ and $\boldsymbol{d}$, i.e. $\boldsymbol{w} = \Delta\boldsymbol{f} + \boldsymbol{d}$, so that Eq. (15) can be written as

$$\begin{aligned} \Delta\dot{\boldsymbol{r}} &= \Delta\boldsymbol{v} \\ \Delta\dot{\boldsymbol{v}} &= \boldsymbol{w} + \Delta\boldsymbol{a} \end{aligned} \tag{16}$$

where $\Delta\boldsymbol{r}$ and $\Delta\boldsymbol{v}$ are the states, $\Delta\boldsymbol{a}$ is the control variable, and $\boldsymbol{w}$ is the disturbance.

For the control to be feasible, the magnitude of the disturbance $|\boldsymbol{w}| = |\Delta\boldsymbol{f} + \boldsymbol{d}|$ must be smaller than the maximum available control acceleration deviation $\Delta\boldsymbol{a}_{\max}$, while $\Delta\boldsymbol{f}$ is proportional to the orbit error. As mentioned, a large orbit error will arise when the reference orbit is updated, and this orbit error is proportional to the degradation of the optical properties. Therefore, both $\Delta\boldsymbol{f}$ and $\boldsymbol{d}$ are proportional to the degradation of the optical properties. Thus, the update rate of the algorithm for the generation of a new reference orbit must be selected appropriately to guarantee that the control is feasible.

4.2. Nonlinear ADRC control law

This ADRC control law consists of a nonlinear extended state observer (ESO), a nonlinear time-optimal feedback law, and an iterative algorithm for solving nonlinear equations. The control laws for the three channels (x, y, and z) are designed independently, and the coupled items are viewed as a disturbance.

Taking the x channel as an example, the nonlinear ESO is given in a discrete form

$$\begin{aligned}
&e_k = \Delta\hat{x}_k - \Delta x_k \\
&\Delta\hat{x}_{k+1} = \Delta\hat{x}_k + h(\Delta\hat{v}_{x,k} - \beta_1 e_k) \\
&\Delta\hat{v}_{x,k+1} = \Delta\hat{v}_{x,k} + h\left(\Delta\hat{w}_{x,k} - \beta_2 \mathrm{fal}\left(e_k, 1/2, h\right) + \Delta a_x\right) \\
&\Delta\hat{w}_{x,k+1} = \Delta\hat{w}_{x,k} + h\left(-\beta_3 \mathrm{fal}\left(e_k, 1/4, h\right)\right)
\end{aligned} \tag{17}$$

where, h is the control period, $\Delta\hat{x}$ and $\Delta\hat{v}_x$ are the estimated deviations of position and velocity relative to the reference orbit in the x-direction, $\hat{w}_x$ is the estimated total disturbance in the x-direction, and β_i (i=1, 2, 3) are the observer gains. The function fal() is defined in Han (2008, 2009), that is

$$\mathrm{fal}(\varepsilon, \tau, \eta) = \begin{cases} \dfrac{\varepsilon}{\eta^{1-\tau}}, & |\varepsilon| \le \eta \\ |\varepsilon|^{\tau}\mathrm{sign}(\varepsilon), & |\varepsilon| > \eta \end{cases} \tag{18}$$

where ε, τ, and η are real numbers.

The required SRP acceleration deviation is given by

$$\Delta a_x = \Delta a_{1,x} - \hat{w}_x \tag{19}$$

with

$$\Delta a_{1,x} = \mathrm{fhan}(\Delta\hat{x}, c_x\Delta\hat{v}_x, \bar{r}_x, \bar{h}_x) \tag{20}$$

where $\bar{r}_x$ is the maximum control acceleration, and c_x and $\bar{h}_x$ are two control parameters. The function fhan() is a nonlinear time-optimal feedback law, which is defined in Han (2008, 2009), that is

$$\begin{cases}
D = \bar{r}\bar{h}^2, A_0 = \bar{h}x_2, Y = x_1 + A_0 \\
A_1 = \sqrt{D(D + 8\,|Y|)}, A_2 = A_0 + \mathrm{sign}(Y)(A_1 - D)/2 \\
s_y = [\mathrm{sign}(Y + D) - \mathrm{sign}(Y - D)]/2 \\
A = (A_0 + Y - A_2)s_y + A_2 \\
s_a = [\mathrm{sign}(A + D) - \mathrm{sign}(A - D)]/2 \\
\mathrm{fhan}(x_1, x_2, \bar{r}, \bar{h}) = -\bar{r}\left[A/D - \mathrm{sign}(A)\right] s_a - \bar{r}\mathrm{sign}(A)
\end{cases} \tag{21}$$

where $x_1, x_2, \bar{r}, \bar{h}, A, A_0, A_1, A_2, D$, and Y are real numbers, while s_y and s_a are integers.

The required SRP acceleration can be obtained by $\boldsymbol{a} = \boldsymbol{a}_e + \Delta\boldsymbol{a}$. However, the real control vector for an RCD solar sail is $\boldsymbol{u} = [\gamma, \delta, \sigma]^T$, i.e. the two sail angles and the RCD ratio. Therefore, the Newton's method is used for mapping $\boldsymbol{a}$ to $\boldsymbol{u}$, i.e., solving the nonlinear system of Eqs. (5–7) for $\boldsymbol{u}$ iteratively with the nominal value $\boldsymbol{u}_e$ as the initial guess.

Figure 7 shows the flow chart of the control loop of the ADRC station-keeping.

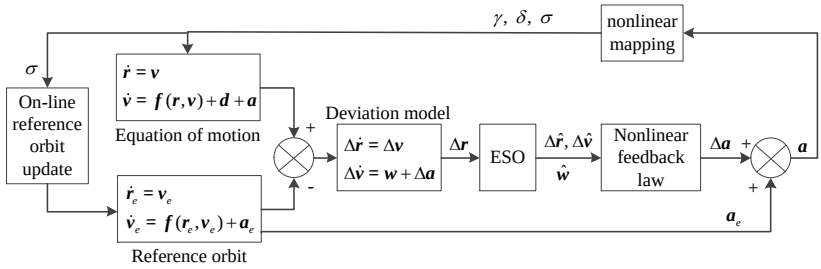

Figure 7: Control loop of the ADRC station-keeping

5. Numerical simulation

In this section, simulations are undertaken in two cases. In the first case, $\beta = 0.056$ and the initial reference orbit with $A_z \approx 0.002$ AU is considered, where A_z is the orbit amplitude in the z-direction. In the second case, $\beta = 0.028$ and the initial reference orbit with $A_z \approx 0.004$ AU is considered. The two initial reference orbits, designed using the nominal sail parameters, are shown in Fig. 8, where Fig. 8a is an orbit in the family of orbits shown in Fig. 6. The initial states of the two initial reference orbit are given by Eqs. (22) and (23),

respectively.

$$\begin{cases} x_0 = 0.975240874297760, \\ z_0 = -0.00213808168231298, \\ v_{y0} = 0.0135800625909357, \\ y_0 = 0, z_0 = 0, v_{x0} = 0, v_{z0} = 0 \end{cases} \tag{22}$$

$$\begin{cases} x_0 = 0.983337296060662, \\ z_0 = -0.00407306209564273, \\ v_{y0} = 0.0118999914581784, \\ y_0 = 0, z_0 = 0, v_{x0} = 0, v_{z0} = 0 \end{cases} \tag{23}$$

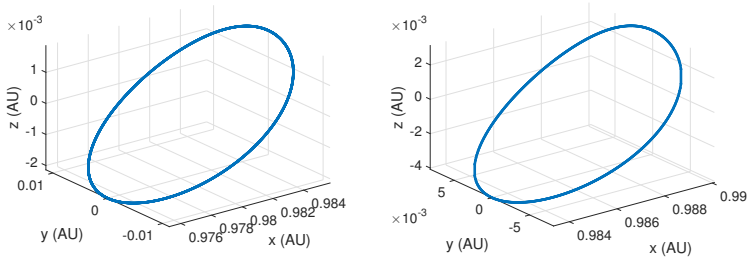

(a) $\beta = 0.056$ and $A_z \approx 0.002$ (b) $\beta = 0.028$ and $A_z \approx 0.004$

Figure 8: Initial reference orbits

The control period h is closely related to the performance of ADRC control. Smaller h can lead to better control accuracy (Han, 2008). However, smaller h also results in the requirements for high-frequency sensors and attitude control, and more power consumption. Therefore, with the precondition of ensuring enough control accuracy, h is chosen as large as possible. For the two cases of simulation in this section, h is set to 0.001 (1.4 hours).

The damping factor c_i and the filter factor $\bar{h}_i$ are the two control parameters whose default values are 1 and h, respectively, which are used in the initial configuration. Increasing c_i can suppress overshoot, while increasing $\bar{h}_i$ can suppress high-frequency oscillation. For the two cases of simulation in this

section, these two parameters are tuned to be $c_i = 1$ and $\bar{h}_i = 5h = 0.005$ $(i = x, y, z)$.

Figure 9 shows the simulation results in the first case without updating the reference orbit in the presence of optical degradation. It can be seen that when the degradation is small the orbit errors and the sail angle deviations remain in the vicinity of zero, while the RCD ratio deviation $\Delta\sigma$ decreases from its nominal value with time to compensate for the degradation of the optical properties. When $\Delta\sigma$ decreases close to its minimum value $\Delta\sigma_{\min} = -0.1$, the position and velocity errors in the x-direction start to diverge. In this simulation, $\Delta\sigma$ decreases to its minimum value after 2.1 years, during which the reflection coefficient ρ is degraded to $0.988\rho_0$. The simulation results in the second case without updating the reference orbit have a similar feature, and are therefore not presented.

The reference orbit is updated when the steady-state $\Delta\sigma$ reaches the minimum prescribed value $\Delta\sigma^*$. The selected value for $\Delta\sigma^*$ depends on several factors: i) the variation of the reference orbit should be small enough to guarantee an effective control; ii) the errors in the optical properties should be small enough to guarantee an effective control; iii) the steady-state $\Delta\sigma$ should not be close to its minimum value. According to the simulation results, the control is effective when $\Delta\sigma^*$ is no smaller than -0.03 in the first case, while in the second case, $\Delta\sigma^*$ must be no smaller than -0.025, where the lightness number is smaller, and thus, less control acceleration is available to compensate for the degradation. In order to make the time interval between two subsequent updates as long as possible, $\Delta\sigma^*$ is set to -0.03 in the first case, and -0.025 in the second case.

The simulation results are demonstrated over a period of five years in both cases, and during this time, ρ is degraded to $0.975\rho_0$ and $0.976\rho_0$, respectively. The control errors and control variables in the two cases are shown in Figs. 10 and 11, respectively. The results in the two cases have similar features. Figures 10a and 11a show that when the reference orbits are updated, large position errors (maximum of 7860 km in the first case, and maximum of 2800 km in the

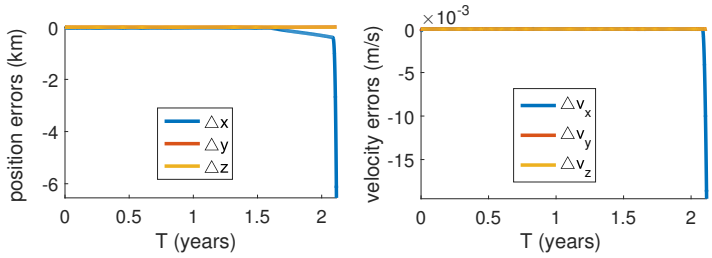

(a) Position errors and velocity errors

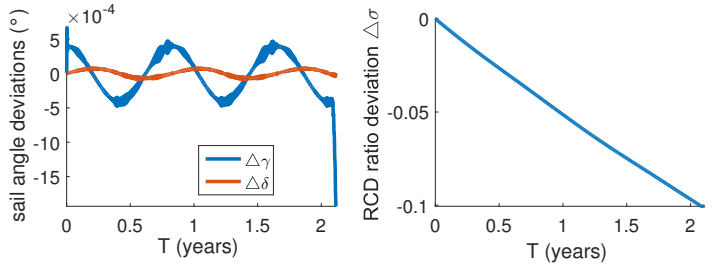

(b) Control variables

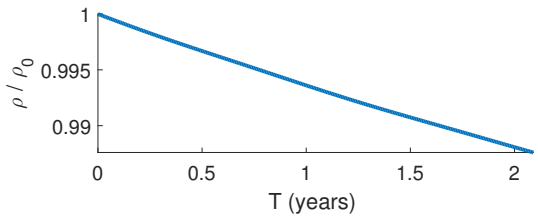

(c) Degradation of ρ

Figure 9: Simulation results without reference orbit update

second case) arise and then converge to zero, and the steady-state errors are close to zero (less than 30 m in the first case, and less than 60 m in the second case). This implies that the ADRC station-keeping control possesses robustness to large orbit errors and high station-keeping accuracy, both requirements of the proposed guidance method.

Figures 10b and 11b show that, when the steady-state $\Delta\sigma$ decrease to $\Delta\sigma^*$, the reference orbits are updated, after which, the steady-state $\Delta\sigma$ jump to a larger value. Therefore, the steady-state $\Delta\sigma$ is always in its available range and

the station-keeping control is always feasible. The simulation orbits in the two cases are shown in Figs. 12 and 13, respectively, which illustrate that the orbits move away from the Sun with time.

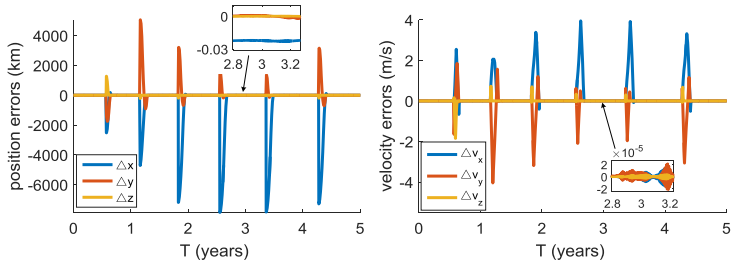

(a) Position errors and velocity errors

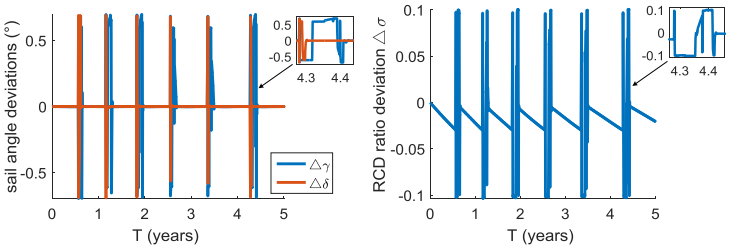

(b) Control variables

Figure 10: Control results with reference orbit update (the first case)

6. Conclusion

This paper has presented an integrated guidance and control strategy for station-keeping of solar sails equipped with reflectivity control devices (RCDs) in the presence of optical degradation. An exponential optical degradation model taking into account the solar radiation dose has been incorporated into the solar radiation acceleration model. In this case, station-keeping without reference orbit updates will fail once the optical properties have degraded by a large amount. To this end, a discrete on-line reference orbit update approach has been incorporated into the station-keeping. The reflection coefficient, which is the major factor affecting the solar radiation acceleration, is estimated on-line,

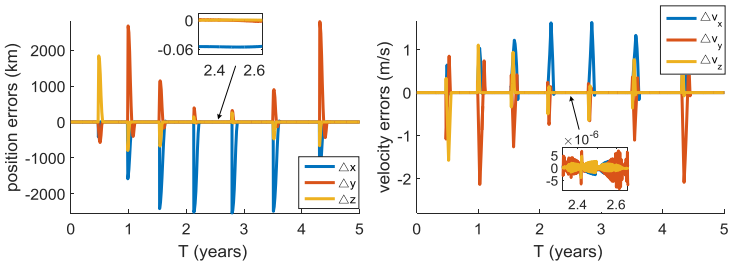

(a) Position errors and velocity errors

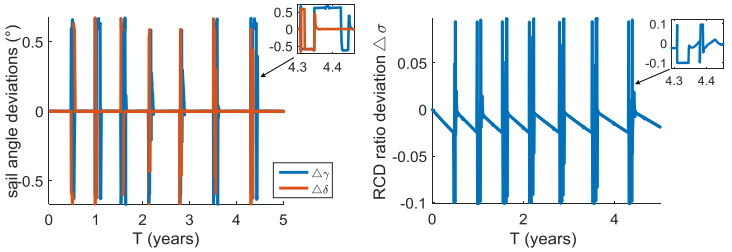

(b) Control variables

Figure 11: Control results with reference orbit update (the second case)

and then the reference orbit is updated using on-line numerical continuation when the optical properties have degraded by a prescribed amount. An active disturbance rejection station-keeping controller has been designed and coupled with the on-line reference orbit update algorithm. Two cases of station-keeping simulations using halo orbits in the Sun-Earth circular restricted three body problem have been performed. The results show that the presented strategy enables a long-term effective station-keeping even in the presence of a large optical degradation. Therefore, the mission time is significantly extended compared to station-keeping that does not utilize guidance-in-the-loop.

Acknowledgments

The authors acknowledge the financial support from the State Administration of Foreign Experts Affairs P. R. China (Grant Number: P180590003).

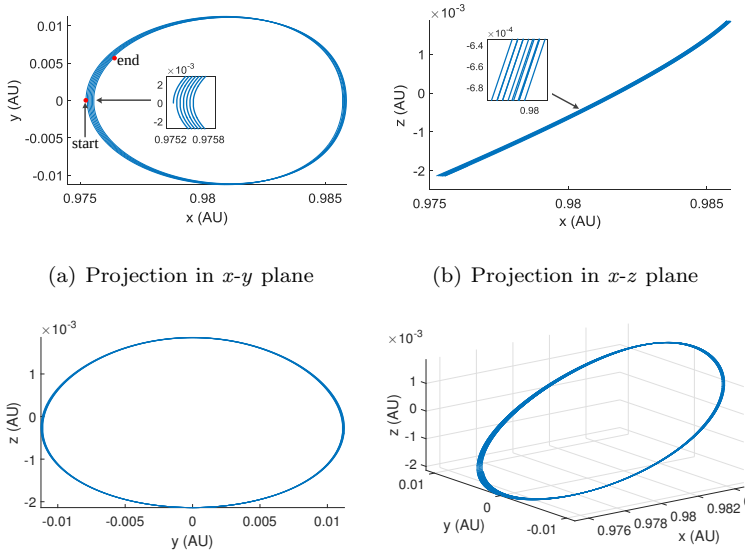

(a) Projection in x-y plane

(b) Projection in x-z plane

(c) Projection in y-z plane

(d) 3-D orbit

Figure 12: Simulation orbit with reference orbit update (the first case)

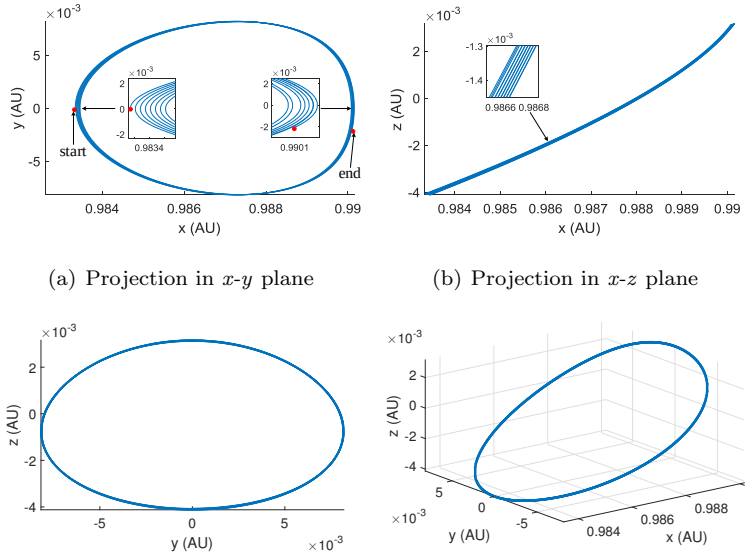

(a) Projection in x-y plane

(b) Projection in x-z plane

(c) Projection in y-z plane

(d) 3-D orbit

Figure 13: Simulation orbit with reference orbit update (the second case)

References

Baoyin, H., McInnes, C.R., 2005. Solar sail orbits at artificial sun-earth libration points. J. Guid. Control Dyn. 28, 1328–1331. doi:https://doi.org/10.2514/1.14598.

Biggs, J.D., Ciccarelli, E., 2019. In-situ tracking of a solar sail's characteristic acceleration using a robust active disturbance estimator. Presented at the 5th International Symposium on Solar Sailing, Aachen, Germany.

Biggs, J.D., McInnes, C.R., 2009. Solar sail formation flying for deep-space remote sensing. J. Spacecraft Rockets 46, 670–678. doi:https://doi.org/10.2514/1.42404.

Biggs, J.D., McInnes, C.R., Waters, T., 2009. Control of solar sail periodic orbits in the elliptic three-body problem. J. Guid. Control Dyn. 32, 318–320. doi:https://doi.org/10.2514/1.38362.

Biggs, J.D., McInnes, C.R., Waters, T., 2011. New periodic orbits in the solar sail three-body problem, in: Nonlinear Science and Complexity. Springer, Dordrecht, pp. 131–138. doi:https://doi.org/10.1007/978-90-481-9884-9_17.

Biggs, J.D., Negri, A., 2019. Orbit-attitude control in a circular restricted three-body problem using distributed reflectivity devices. J. Guid. Control Dyn. doi:https://doi.org/10.2514/1.G004493. (in press).

Ceriotti, M., McInnes, C.R., 2012. Natural and sail-displaced doubly-symmetric lagrange point orbits for polar coverage. Celest. Mech. Dyn. Astr. 114, 151–180. doi:https://doi.org/10.1007/s10569-012-9422-2.

Dachwald, B., Macdonald, M., McInnes, C.R., Mengali, G., Quarta, A.A., 2007. Impact of optical degradation on solar sail mission performance. J. Spacecraft Rockets 44, 740–749. doi:https://doi.org/10.2514/1.21432.

Dachwald, B., Mengali, G., Quarta, A.A., Macdonald, M., 2006. Parametric model and optimal control of solar sails with optical degradation. J. Guid. Control Dyn. 29, 1170–1178. doi:https://doi.org/10.2514/1.20313.

Funase, R., Shirasawa, Y., Mimasu, Y., Mori, O., Tsuda, Y., Saiki, T., Kawaguchi, J., 2011. On-orbit verification of fuel-free attitude control system for spinning solar sail utilizing solar radiation pressure. Adv. Space Res. 48, 1740–1746. doi:https://doi.org/10.1016/j.asr.2011.02.022.

Gong, S., Li, J., 2014. Solar sail heliocentric elliptic displaced orbits. J. Guid. Control Dyn. 37, 2021–2026. doi:https://doi.org/10.2514/1.G000660.

Gong, S., Li, J., Simo, J., 2014. Orbital motions of a solar sail around the L2 earth–moon libration point. J. Guid. Control Dyn. 37, 1349–1356. doi:https://doi.org/10.2514/1.G000063.

Grebow, D.J., Ozimek, M.T., Howell, K.C., 2010. Advanced modeling of optimal low-thrust lunar pole-sitter trajectories. Acta Astronaut. 67, 991–1001. doi:https://doi.org/10.1016/j.actaastro.2010.04.024.

Han, J., 2008. Active Disturbance Rejection Control Technique: the Technique for Estimating and Compensating the Uncertainties. National Defense Industry Press, Beijing, China. (in Chinese).

Han, J., 2009. From PID to active disturbance rejection control. IEEE T. Ind. Electron. 56, 900–906. doi:https://doi.org/10.1109/TIE.2008.2011621.

Heaton, A., Ahmad, N., Miller, K., 2017. Near earth asteroid scout solar sail thrust and torque model, in: Proceedings of the 4th International Symposium on Solar Sailing, Kyoto, Japan. p. 17055. URL: http://www.jsforum.or.jp/ISSS2017/papers/.

Heiligers, J., Diedrich, B., Derbes, B., McInnes, C., 2014. Sunjammer: preliminary end-to-end mission design, in: Proceedings of the AIAA/AAS Astrodynamics Specialist Conference, AIAA 2014-4127, San Diego, CA, USA. doi:https://doi.org/10.2514/6.2014-4127.

Heiligers, J., Macdonald, M., Parker, J.S., 2016. Extension of earth-moon libration point orbits with solar sail propulsion. Astrophys. Space Sci. 361, 241. doi:https://doi.org/10.1007/s10509-016-2783-3.

Heiligers, J., McInnes, C.R., Biggs, J.D., Ceriotti, M., 2012. Displaced geostationary orbits using hybrid low-thrust propulsion. Acta Astronaut. 71, 51–67. doi:https://doi.org/10.1016/j.actaastro.2011.08.012.

Heiligers, J., Vergaaij, M., Ceriotti, M., 2019. End-to-end trajectory design for a solar-sail-only pole-sitter at Venus, Earth, and Mars. Presented at the 5th International Symposium on Solar Sailing, Aachen, Germany.

Howell, K.C., 1984. Three-dimensional, periodic,'halo' orbits. Celestial Mech. 32, 53–71. doi:https://doi.org/10.1007/BF01358403.

Huang, J., Biggs, J.D., Cui, N., 2019. Families of halo orbits in the elliptic restricted three-body problem for a solar sail with reflectivity control devices. Adv. Space Res. doi:https://doi.org/10.1016/j.asr.2019.10.010. (in press).

Lawrence, D., Piggott, S., 2004. Solar sailing trajectory control for sub-L1 stationkeeping, in: Proceedings of the AIAA Guidance, Navigation, and Control Conference and Exhibit, AIAA-2004-5014, Providence, Rhode Island. doi:https://doi.org/10.2514/6.2004-5014.

Macdonald, M., Hughes, G., McInnes, C., Lyngvi, A., Falkner, P., Atzei, A., 2006. Solar polar orbiter: a solar sail technology reference study. J. Spacecraft Rockets 43, 960–972. doi:https://doi.org/10.2514/1.16408.

McInnes, C.R., 1999. Solar sailing: technology, dynamics and mission applications. Springer and Praxis, Chichester, UK.

Negri, A., Biggs, J.D., 2019. Attitude tracking of a solar sail using pixelated reflectivity control devices. Presented at the 5th International Symposium on Solar Sailing, Aachen, Germany.

Waters, T.J., McInnes, C.R., 2008. Invariant manifolds and orbit control in the solar sail three-body problem. J. Guid. Control Dyn. 31, 554–562. doi:https://doi.org/10.2514/1.32292.

Yen, C.L., 2004. Solar sail geostorm warning mission design, in: Proceedings of the 14th AAS/AIAA Space Flight Mechanics Conference, AAS 04-107, Hawaii.